

XMM-NEWTON SURVEY OF THE CHAMAELEON I STAR FORMING REGION

A. Telleschi¹, M. Güdel¹, K. Briggs¹, and M. Audard²

¹Paul Scherrer Institut, Würenlingen und Villigen, CH-5232 Villigen PSI, Switzerland

²Columbia Astrophysics Laboratory, Mail code 5247, 550 West 120th Street, New York, NY 10027, USA

ABSTRACT

We present results of an *XMM-Newton* survey of the Chamaeleon I star forming region. In the five exposures we detected a total of 449 X-ray sources. Among them 96 are counterparts to the 138 spectroscopically confirmed members in the surveyed region; six of them have a spectral type later than M6.5 and are therefore classified as brown dwarfs. The spectra of the brighter sources were analyzed using a continuous emission-measure model composed of two power laws in temperature, as suggested from high-resolution X-ray spectroscopy. We investigate correlations between the derived X-ray luminosity and stellar properties such as rotation rate, mass and bolometric luminosity. We find a deviation from the galactic N_H/A_J relation in Chamaeleon I that could be explained with a larger characteristic dust-grain size.

Key words: Chamaeleon I; Star forming region; X-rays.

1. INTRODUCTION

X-ray surveys play a crucial role in the study of high-energy radiation processes relevant to star and planet formation. Young stars, independently of their accretion rate, are very strong X-ray emitters.

The Chamaeleon I cloud is one of the nearest and best studied star forming regions at a distance of about 160 pc (Whittet et al., 1997). Its high galactic latitude ($b \approx -16^\circ$) minimizes the number of foreground and background stars, and its compactness allows the cloud to be surveyed by only a few *XMM-Newton* observations.

Our survey is based on five *XMM-Newton* observations that are shown in Figure 1 and summarized in Table 1. Using the maximum likelihood detection algorithm *eboxdetect* and *emldetect* within the *XMM Newton* SAS software, a total of 449 X-ray sources were detected in the five fields. Using the works of Luhman 2004 (optical spectroscopy), Comeron et al. 2004 ($H\alpha$ emission and spectroscopy) and Gomez & Mardones 2003 (NIR spectroscopy), we cross-identified our X-ray source catalog with the 138 known Chamaeleon I members in our

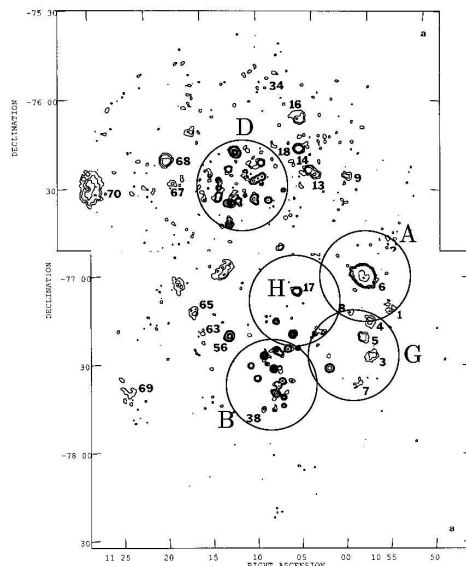


Figure 1. ROSAT contour map of the Chamaeleon I star forming region adapted from Feigelson et al. (1993; reproduced with permission of the AAS) with the five XMM-Newton EPIC fields overlaid.

Table 1. Observation log for the 5 Chamaeleon I fields

Field	Pointing RA	Pointing dec	Exposure [sec]
A	10:59:07.10	-77:01:49.0	35423
B	11:07:52.90	-77:36:56.0	31122
D	11:11:30.00	-76:31:00.0	26035
G	11:00:06.00	-77:28:51.0	29034
H	11:06:05.00	-77:10:40.0	28834

observation fields. Of the X-ray sources, 96 are identified with Chamaeleon I members.

2. MODEL FOR SPECTRAL FIT

Low-resolution spectra are often fitted using a 1-, 2- or 3-temperature model. From high-resolution spectroscopy, however, it has become evident that coronae display continuous emission measure distributions (EMD). The derivation of a continuous EMD is more ambiguous from low resolution spectra such as those from the EPIC spectra. From a physical point of view, coronal, magnetically trapped plasma are also expected to be arranged in continuous EMDs. We therefore build a simple model using the knowledge on EMD derived from high-resolution spectroscopy. In our work on high-resolution spectroscopy of young solar mass stars (Telleschi et al., 2005), we found that in most cases the EMD has a structure that can be approximated by two power laws on each side of a peak. The continuous emission-measure model used to fit the Chamaeleon I members is composed of two power laws in temperature and is given by the formula:

$$Q(T) = \begin{cases} EM_0 \cdot (T/T_0)^\alpha & , \text{for } T \leq T_0 \\ EM_0 \cdot (T/T_0)^\beta & , \text{for } T > T_0 \end{cases} \quad (1)$$

where T_0 is the temperature at the EMD peak and EM_0 is its emission measure. The slope of the power law below T_0 is α , whereas β is the power-law slope above T_0 . We introduce a low-temperature and an high-temperature cutoff, fixed at $\log T = 6.0$ and $\log T = 8.0$, respectively. We also fixed α at a value of 2, consistent with EMD slopes for young stars as found from high-resolution spectroscopy (see for example Argiroffi et al. 2004 and Telleschi et al. 2005). Guided by the coronal element abundances found in the literature (Scelsi et al. 2004, Argiroffi et al. 2004, Garcia-Alvarez et al. 2005 and Telleschi et al. 2005) we adopted an abundance pattern typical for young stars. These abundances are plotted in Figure 2 relative to oxygen, as a function of the first ionization potential (FIP). The distribution is thus one signifying a clear *inverse FIP-effect*. We fitted all, except some very faint, sources in our five fields using this model, obtaining a homogeneous set of X-ray properties that can be used for studies of correlation with other stellar parameters.

3. RESULTS

3.1. The rotation-activity relation

In Figure 3 we plot L_X/L_{bol} as a function of the rotation period P_{rot} . We divide our stellar population in two sub-populations, the Classical T Tauri Stars (CTTS) that show

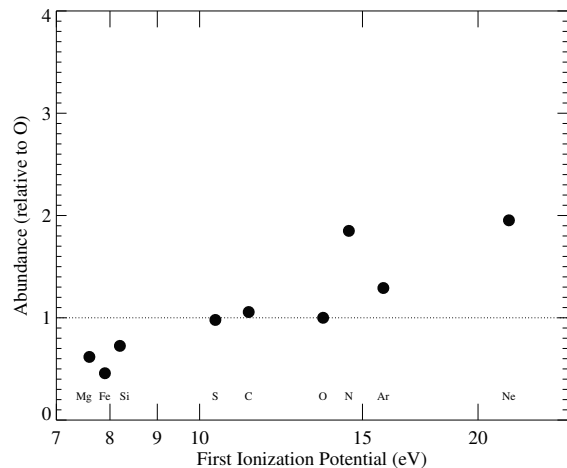


Figure 2. Abundances used in the EMD model, relative to the oxygen abundance, as a function of the FIP. Abundances are normalized to solar photospheric values (Anders & Grevesse, 1989). The abundance of oxygen is 0.426.

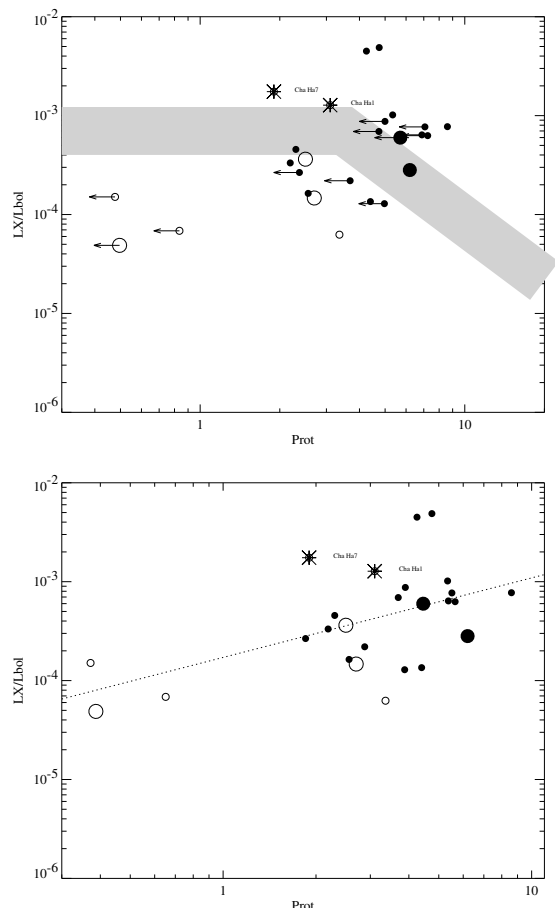


Figure 3. L_X/L_{bol} as a function of the rotation period. Big circles are CTTS and small circles are WTTS. The crosses mark the BDs. The open circles are faint sources, with less than 100 cts in the spectrum. Arrows indicate upper limits for P_{rot} derived from the $vsini$ values.

evidence for strong accretion such as broad $H\alpha$ emission lines, and the Weak-lined T Tauri Stars (WTTS), that show only very weak $H\alpha$ emission. We used the $H\alpha$ equivalent widths from Luhman (2004) and references therein. Big and small circles represent CTTS and WTTS, respectively. Filled circles are bright sources with more than 100 counts, whereas empty circles are sources with less than 100 counts in the fitted spectrum. The asterisks mark the two Brown Dwarfs (BD) for which the rotation period is known. On the upper plot the arrows indicate upper limits to the rotation periods that we derived from the $v\sin i$ values. The grey bar represents an average rotation-activity relation for main-sequence stars. This relation was empirically derived from the work of Pizzolato et al. (2003): the locus for the kink was calculated for K7-M0 main-sequence stars, equivalent to stars with a bolometric luminosity of $\approx 0.1L_{\odot}$. In Chamaeleon I we do not find a trend of decreasing L_X/L_{bol} for slower rotators. On the contrary, as shown in Figure 3 below, if we fit our data with a regression line, we find that L_X/L_{bol} increases for higher rotation periods. The regression line has a slope of 0.8 and is described by the relation $\log(L_X/L_{bol}) = -3.77(\pm 0.26) + 0.80(\pm 0.15) \cdot \log P_{rot}$. A similar trend was found in Orion by Preibisch et al. (2005): they found a slope of 1.27 and a linear regression $\log(L_X/L_{bol}) = -4.21(\pm 0.07) + 1.27(\pm 0.09) \cdot \log P_{rot}$. In contrast, Güdel et al. (2005) find for the Taurus Molecular Cloud a relation similar to the main sequence relation, with decreasing L_X/L_{bol} for longer rotation periods.

Unfortunately, in Cha I, the number of known rotation periods is small and the statistics is not sufficient to draw firm conclusions about the activity-rotation relation. We can state however, that no appreciable drop of L_X/L_{bol} is visible in the range of $P_{rot} = 5 - 10$ days.

3.2. The L_X/L_{bol} relation

In Figure 4 the X-ray luminosity is plotted as a function of the bolometric luminosity. Overplotted are the three lines for $L_X/L_{bol} = 10^{-4}$, $L_X/L_{bol} = 10^{-3}$, and $L_X/L_{bol} = 10^{-2}$. We note that nearly all low mass stars ($M < 2M_{\odot}$) have $L_X/L_{bol} > 10^{-4}$. Although the *detected* brown dwarfs (asterisks) are higher in L_X/L_{bol} (mean value above 10^{-3}) than low-mass stars (mean value of $10^{-3.3}$), the upper limits of undetected brown dwarfs fill the space below the detected ones. Thus we conclude that brown dwarfs are likely to follow the same trend as low mass stars in Chamaeleon I.

In order to estimate the mean value of L_X/L_{bol} for the two populations of CTTS and WTTS we plot histograms for $\log L_X/L_{bol}$ and fit the resulting distribution with a Gaussian. As shown in Figure 5, we find a mean value for $\log L_X/L_{bol}$ of approximately -3.3 for both CTTS and WTTS. We conclude that there is no global influence of the accretion behavior on the X-ray output of T Tau stars in ChaI.

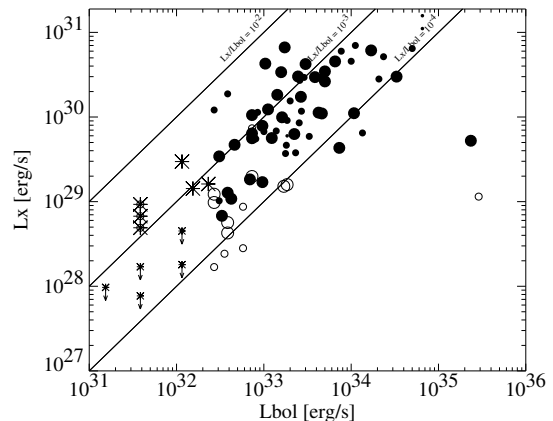


Figure 4. X-ray luminosity as a function of the bolometric luminosity. Key to the symbols: Size, from largest to smallest: CTTS - WTTS - unknown class. Asterisks are BDs. Asterisks with arrows are upper limits for undetected BDs. The open circles are faint sources, with less than 100 cts in the spectrum.

3.3. The mass-activity relation

In Figure 6 the X-ray luminosity is plotted as a function of the logarithm of the stellar mass. The masses are derived from the effective temperature and the bolometric luminosity using the isochrones of Siess et al. (2000) for masses larger than $0.1 M_{\odot}$ and from Chabrier et al. (2000) for smaller masses. It is evident that $\log L_X$ increases with mass. The dash-dotted line describes the linear regression fit obtained by considering the stars between 0.1 and $2 M_{\odot}$ (i.e. excluding the brown dwarfs). This regression line has a slope of 1.31 and is described by $\log L_X = 30.32(\pm 0.1) + 1.31(\pm 0.2) \cdot \log(M/M_{\odot})$. We notice that the relation does not seem to be linear but is flatter for stars with higher masses. Again the BDs (detected and upper limits) fit well in the stellar relation. An X-ray luminosity-mass correlation was already found by Feigelson et al. (1993) in Chamaeleon I. In that study, based on ROSAT observations, a much steeper slope of 3.6 was found for the same correlation. Our dependence is, however, similar to the one found for the Orion Nebula Cluster by Preibisch et al. (2005), where a slope of 1.44 was reported.

3.4. The N_H/A_J relation

We plot in Figure 7 the hydrogen column density N_H as a function of the infrared extinction A_J . In order to avoid effects from circumstellar material we concentrate in this study only on WTTS. The two thin lines are theoretical values for the N_H/A_J relation valid for the interstellar medium, and they are calculated as follows. The ratio N_H/A_V is taken from the literature: $N_H/A_V = 1.8 - 2.2 \times 10^{21} \text{cm}^{-2}/\text{mag}$. We then used the Cardelli et al. (1989) extinction law, for which the A_J/A_V relation

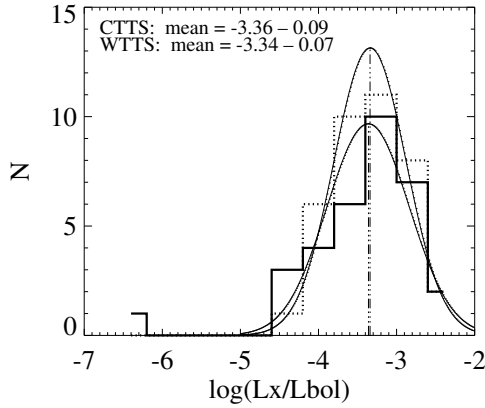


Figure 5. Histogram for L_X/L_{bol} . Solid histogram is for WTTs, dashed histogram is for CTTS.

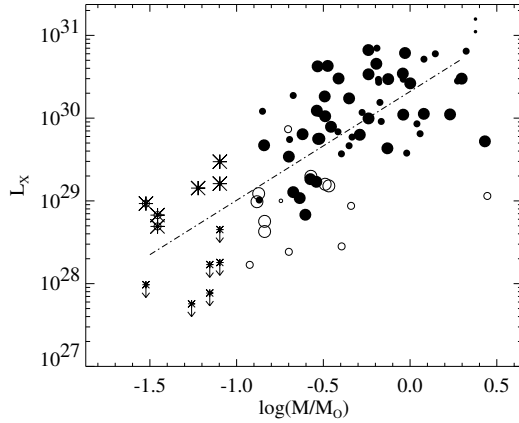


Figure 6. X-ray luminosity as a function of the stellar mass. Symbols as in Figure 4.

depends only on one parameter, $R_V = A_V/(A_B - A_V)$, and is described by the formula

$$A_J/A_V = 0.4008 - 0.3679/R_V. \quad (2)$$

The galactic value for R_V is found to be 3.1. Using this relation, we obtain

$$(N_H/A_J)_{gal} = 6.4 - 7.8 \times 10^{21} \text{ cm}^{-2}/\text{mag}. \quad (3)$$

This N_H/A_J range is plotted as a black line in both Figures 7. We see that in Cha I many stars lie on a line that indicates reduced N_H . This line is represented by the thick line that fits the relation

$$N_H/A_J = 4.1 \times 10^{21} \text{ cm}^{-2}/\text{mag}. \quad (4)$$

A deviation from the galactic value of N_H/A_J was also found and studied in detail by Vuong et al. (2003) for the star-forming region ρ Oph. They obtained $N_H/A_J = 5.57 \times 10^{21} \text{ cm}^{-2}/\text{mag}$, using the Cardelli et al. (1989) A_J/A_V relation. In their work the measured N_H/A_J

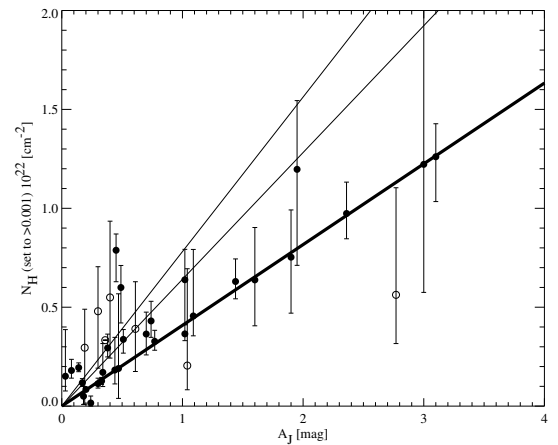
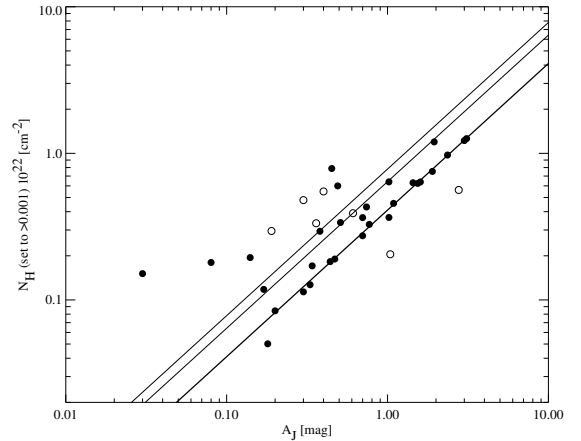


Figure 7. Hydrogen column density, N_H , as a function of the infrared extinction, A_J . The two thin black lines are values from the literature (see text). Note that only WTTs are plotted.

value was used in a physical model of gas and dust properties to constrain the grain size distribution and the gas-to-dust ratio. They found a bigger mean grain size ($\langle a \rangle = 0.035 - 0.095 \mu\text{m}$ instead of $\langle a \rangle = 0.008 \mu\text{m}$) and a gas-to-dust mass ratio of 80-95.

In Chamaeleon, this model cannot be used, because the N_H/A_J ratio is too small to derive a reasonable value for R_V using the Cardelli et al. (1989) extinction curves (note that higher R_V values were already claimed in Cha I, see for example Whittet et al. 1997 and Luhman 2004). However, we can state that this deviation from $(N_H/A_J)_{gal}$ is in the same direction of the deviation found by Vuong et al. (2003) and would also predict a higher R_V value and a larger characteristic mean grain size. As the gas-to-dust ratio strongly depends on both R_V and N_H/A_J in the model, we are not able to predict the variation of gas-to-dust mass ratio in our case.

3.5. Summary and conclusions

In the five *XMM-Newton* observations of the Chamaeleon I region we detected 96 cloud members. Of them, 6 are considered brown dwarfs. We correlated the X-ray activity, i.e. the ratio between X-ray luminosity and bolometric luminosity, with the rotation period, but we could not find any decrease in activity for slower rotators, as it is found for main sequence stars. This result could be evidence for long convective turnover times in our sample of stars. We further studied the relation between X-ray luminosity and bolometric luminosity and found that almost all low-mass stars have a ratio $\log L_X / \log L_{bol}$ between -4 and -2 , with a mean value at -3.3 for both CTTS and WTTS. We concluded that there is no influence of accretion on the X-ray output. An evident increase of L_X with the stellar masses is also found. Brown dwarfs do not show exceptional properties, but fit well to all the studied correlations. Finally, we investigated the ratio between the hydrogen column density N_H and the infrared extinction A_J . We found $N_H/A_J = 4.1 \times 10^{21} \text{cm}^{-2}/\text{mag}$, much lower than the galactic value $N_H/A_J = 6.4 - 7.8 \times 10^{21} \text{cm}^{-2}/\text{mag}$ valid for the interstellar medium. This deviation is too large to draw quantitative conclusions about the gas-to-dust ratio, but we can qualitatively affirm that deviations on the same direction could be modeled with a larger characteristic mean grain size of the dust.

ACKNOWLEDGMENTS

We acknowledge support from NASA grants NNG04GF72G and NNG04GE65G, and from grant 20-66875.01 from the Swiss National Science Foundation. Based on observations obtained with *XMM-Newton*, an ESA science mission with instruments and contributions directly funded by ESA Member States and NASA.

REFERENCES

- Anders, E., & Grevesse, N., *Geochim. Cosmochim. Acta*, 53, 197
- Argiroffi, C., Drake, J.J., Maggio, A., Peres, G., Sciortino, S., Harnden F.R. 2004, *ApJ*, 609, 925
- Cardelli, J., Clayton, G., Mathis, J. 1989 *ApJ*, 467,334
- Chabrier, G., Baraffe, I., Allard, F., Hauschildt, P. 2005, *ApJ*, 621, 1009
- Comeron, F., Reipurth, B., Henry, A., Fernandez, M. 2004, *A&A*, 417, 583
- Feigelson, E.D., Casanova S., Montmerle, T., Guiubert, J. 1993, *ApJ*, 416, 623
- Garcia-Alvarez, D., Drake, J.J., Lin, L., Kashyap, V.L., Ball, B. 2005, *ApJ*, 621, 1009
- Gomez, M., & Mardones, D. 2003 *AJ*, 125, 2134
- Güdel et al. 2005, *The X-ray Universe 2005*
- Luhman, K.L. 2004, *ApJ*, 602, 816
- Pizzolato, N., Maggio, A., Micela, G. Sciortino, S., Ventura, P. 2003, *A&A*, 397, 147
- Preibisch, T., Kim, Y.-C., Favata, F, Feigelson, E., D., Flaccomio, E., Micela, G., Sciortino, S., Stassun, K., Stelzer, B., Zinnecker, H., *ApJ*, submitted
- Scelsi, L., Maggio, A., Peres, G., Pallavicini, R. *A&A*, 2005 432, 671
- Siess, L., Dufour, E., Forestini, M. 2000, *A&A*, 358, 593
- Telleschi, A., Güdel, M., Briggs, K., Audard, M., Ness, J.-U., Skinner, L.S. 2005, *ApJ*, 622, 653
- Vuong, M.H., Montmerle, T., Grosso, N., Feigelson E.D., Verstraete, L., Ozawa, H. 2003 *A&A*, 408, 581
- Whittet, D.C.B., Prusti, T., Franco, G.A.P. et al. 1997, *A&A*, 327, 1194